

Two-Dimensional Compact FD-Like Stencils with High-Order Accuracy for Helmholtz Equation with a Planar Dielectric Interface

Hung-Wen Chang* and Sin-Yuan Mu

Abstract—We derive and compare several finite-difference frequency-domain (FD-FD) stencils for points on or near a planar dielectric interface. They are based on interface conditions or from modifying Helmholtz equation. We present a highly accurate formulation based on local plane wave expansion (LPWE). LPWE-based compact stencil is an extension of the analytically obtained LFE-9 stencil as used by the method of connected local fields [6]. We report that merely using five points per wavelength spatial sampling, LPWE coefficients achieve better than 0.01% local error near a planar interface. We numerically determine that we have fourth to eighth-order accuracy in the local errors for LPWE stencils.

1. INTRODUCTION

Numerical solutions of Helmholtz equation by the classical second-order accurate finite-difference (FD) method have been investigated. Solutions of classical high-accuracy FD approximations to Helmholtz equation can be realized by non-compact stencils at the expense of increased computational costs. Having a compact stencil which only connects a point of interest to its neighboring eight points is one of the critical factors of success for the frequency-domain FD method. Compact stencils produce block tri-diagonal matrices that require much less computing resources than non-compact stencils.

Over the last two decades, many high-order compact formulae for discretizing 2-D and 3-D homogeneous Helmholtz equation have been proposed. In particular, the sixth-order accurate (the highest possible order of accuracy) compact 2D formulae were published by various research groups [1–4]. Both Hadley [5] and Chang-Mu [6] used Fourier-Bessel series expansion (FBSE) for the local field in deriving a 2D compact FD-like formula, which we refer to as LFE-9. Along these lines, Tsukerman [3] proposed other choices of basis functions for 2D Helmholtz equation including plane waves and harmonic polynomials. He called this new class of difference schemes FLAME (Flexible Local Approximation Methods).

The method of connected local fields (CLF) [6–9] is a new approach for obtaining semi-analytical solutions of Helmholtz equation. In 2D-CLF, the global solution is comprised of overlapping local fields. Each local field (patch) is represented by a truncated Fourier-Bessel Series, in which each individual term precisely satisfies Helmholtz equation. CLF connects these patches of local fields and forms a system of linear equations just like the standard FD-FD method.

Frequency-domain finite-difference (FD-FD) methods have been successfully applied to study 2D passive dielectric waveguide devices with high index contrasts [10–12]. Semivectorial modes of optical waveguides are also studied by classical FD methods [13–15]. For media with sudden jumps in material properties, special compact stencils are needed for points on/near a dielectric interface. For performance and storage considerations, most commercial FD-TD software use stair-case approximations for the underlying structure [16, 17]. The coefficients for a point near an interface are determined by the

Received 18 August 2015, Accepted 26 October 2015, Scheduled 2 November 2015

* Corresponding author: Hung-Wen Chang (hchang@mail.nsysu.edu.tw).

The authors are with the Department of Photonics, National Sun Yat-sen University, Kaohsiung 80424, Taiwan, R. O. C..

material properties sampled at the point location. The sampled area surroundings form an artificially generated jagged boundary [18], which result in undesired numerical errors. This phenomenon is even more noticeable when modeling optical waveguide devices with large index contrasts. The stair-case approximation of the underlying dielectric structure by the FD-TD method will converge to a valid solution (as the discretization approaches zero) because FD-TD method is based on the first-order Maxwell's PDE, hence its unknowns sitting on or near dielectric interfaces will automatically satisfy the interface conditions. However, the standard FD-FD method is based on the second-order Helmholtz PDE. The stair-case approximation of the underlying structure properties will not work since the resulting FD-FD coefficients are the same for both TE and TM polarizations no matter how small the grid spacing becomes. Customized FD-FD coefficients based on interface conditions are needed for points near or on the interfaces between two dielectric materials. Some early researches on the FD coefficients for points near or on the interfaces are briefly summarized in Durdević's work [19].

While we are able to obtain analytical formula for compact FD coefficients in homogeneous media using FBSE technique, we had to resort to the numerical approach to compute desired stencils for materials with abrupt changes in dielectric constants. In this paper we only consider planar dielectric interface cases. In the next section, we will first give an overall description for discretizing the 2D Helmholtz interface problem, we then review several kinds of FD-like formulae. This highly accurate scheme for planar interface problems — the Local Plane Wave Expansion (LPWE) formulation will be developed in detail in Section 3. To evaluate the performance of the LPWE scheme, we compare its relative local error to other FD-like formulae in Section 4. Finally, we present the tabulated characteristics of the LPWE scheme versus other FD-like formulation in Section 5.

2. FD-LIKE SCHEMES FOR INTERFACE PROBLEMS

For pure 2-D electromagnetic (EM) wave problems, all field components and material indices are assumed to only be functions of x and y , and the solutions to 2-D EM problems can be divided into z -polarized TE and z -polarized TM waves [20]. The FD compact nine-point stencil with an arbitrarily positioned inclined planar interface is depicted in Fig. 1, where medium 1 (with index n_1) is separated from medium 2 (with index n_2) by the straight line L , whose equation can be expressed as:

$$a(x/\Delta) + b(y/\Delta) + c = 0. \quad (1)$$

Now we use the interface-oriented coordinate system $x'-y'$ shown in Fig. 1 to formulate the interface EM problem, which is governed by the following 2-D Helmholtz equation with piecewise-constant

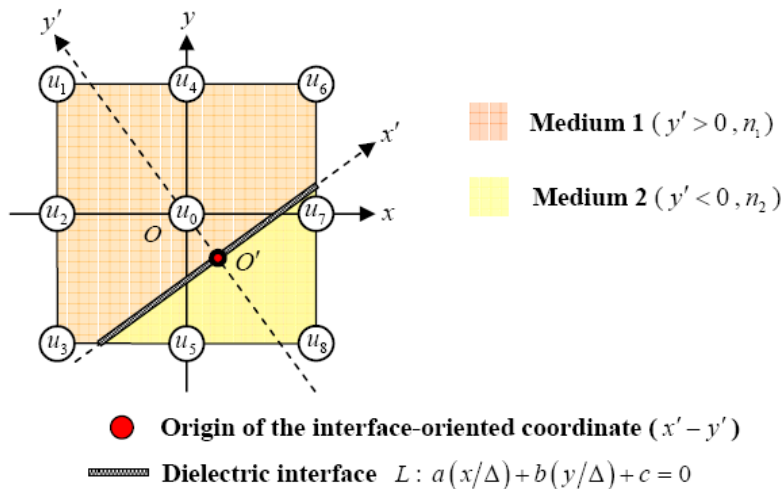


Figure 1. A 2D compact nine-point stencil with an arbitrarily located inclined planar dielectric interface separating medium 1 (marked in orange) from medium 2 (marked in yellow). The x and y -spacing between adjacent points are both Δ .

wavenumbers:

$$\left(\partial^2/\partial x'^2 + \partial^2/\partial y'^2 + k_i^2\right) u(x', y') = 0, \quad i = 1 \text{ for } y' > 0 \text{ and } i = 2 \text{ for } y' < 0. \quad (2)$$

In Eq. (2), $k_i = n_i k_0$ ($i = 1, 2$), and $k_0 = \omega/c$. The function u denotes E_z for TE case, and H_z for TM case. In addition, continuity requirements of both the tangential electric and magnetic fields, u lead to the following interface conditions:

$$(i) \ u(x', y' = 0^+) = u(x', y' = 0^-), \quad (3)$$

$$(ii) \ \partial u/\partial y'|_{y'=0^+} = \gamma \cdot \partial u/\partial y'|_{y'=0^-}. \quad (4)$$

In Eq. (4), the polarization parameter γ is defined as:

$$\gamma = \begin{cases} 1, & \text{TE} \\ n_1^2/n_2^2, & \text{TM} \end{cases}. \quad (5)$$

Note that the primed coordinate (x', y') is related to the unprimed coordinate (x, y) by Eq. (6):

$$\mathbf{r} - \mathbf{d}_0 = \mathbf{r}' \Leftrightarrow \begin{bmatrix} x \\ y \end{bmatrix} = \frac{1}{\sqrt{a^2 + b^2}} \begin{bmatrix} b & a \\ -a & b \end{bmatrix} \begin{bmatrix} x' \\ y' \end{bmatrix} - \frac{c}{a^2 + b^2} \begin{bmatrix} a \\ b \end{bmatrix} \cdot \Delta, \quad (6)$$

where $\mathbf{r} = \hat{x}x + \hat{y}y$, $\mathbf{d}_0 = \overrightarrow{OO'}$, and $\mathbf{r}' = \hat{x}'x' + \hat{y}'y'$. Our goal is to derive a compact FD-like formulation to express the central field u_0 as a linear combination of the eight neighboring sampled fields sitting on the square cell. The compact FD-like formula for discretizing the 2-D Helmholtz equation can be expressed in the general form:

$$u_0 = \sum_{i=1}^8 w_i \cdot u_i = \mathbf{u}_c^T \mathbf{w}, \quad (7)$$

where the control (neighboring) point vector $\mathbf{u}_c = [u_1, u_2, \dots, u_8]^T$, and the coefficient vector $\mathbf{w} = [w_1, w_2, \dots, w_8]^T$. In general, the coefficients are dependent on the refractive indices n_1, n_2 , frequency ω , sampling spacing Δ and the interface parameters a, b, c . In the following subsections, 2.1, 2.2, 2.3, and 2.4, we review several compact FD-like schemes for discretizing the interface problem for the specific interface type where $(x', y') \equiv (x, y)$ and $(a, b, c) = (0, 1, 0)$.

2.1. Formula Based on FD Approximations of Interface Conditions (CmptHIC)

Discretization of the interface conditions can be intuitively implemented by finite difference approximations. The first interface condition, shown in Eq. (3), is automatically satisfied when $(a, b, c) = (0, 1, 0)$. For the second interface condition, as shown in Eq. (4), we approximate the upper and lower halves by correspondingly applying forward and backward difference operators, resulting in the following compact formulae based on horizontal interface conditions:

$$u_0 = 1/(1 + \gamma) \cdot u_4 + 1/(1 + 1/\gamma) \cdot u_5 \quad (\text{CmptHIC}) \quad (8)$$

2.2. FD Approximation of Helmholtz Equation and Material Averaging (FD-MatAve)

A widely accepted approach for handling interfaces is to adopt a material-averaging (MatAve) scheme, which is similar to the effective index method in the modeling of 3D complex dielectric waveguides [16, 17]. We have considered and published a polarization-dependent material averaging method for a hybrid 2D FD-FD method [10–12]. In this approach, we do not rigorously handle geometric variations of the material structure. The effective refractive index at the heterogeneous junction is defined by averaging the material permittivities as given in Eq. (9).

$$n(y = 0) \triangleq n_{\text{avg}} = \sqrt{(n_1^2 + n_2^2)/2}. \quad (9)$$

Approximating Eq. (2) for the central field u_0 with the help of Eq. (9), we have

$$[3 + (1/\gamma + \gamma)/2 - n_{\text{avg}}^2 V_0^2] u_0 = u_2 + (1 + 1/\gamma)/2 \cdot u_4 + (1 + \gamma)/2 \cdot u_5 + u_7. \quad (\text{FD-MatAve}) \quad (10)$$

In Eq. (10), $V_0 = k_0 \cdot \Delta$, which is called the normalized frequency in vacuum.

2.3. FD Approximation of Helmholtz Equation by Arbitrary-Order Interface Conditions (FD-AIC)

In the material-averaging scheme, the difference formula for the normal partial derivative is only a first-order approximation due to the presence of the interface. Based on Chiou's work [21, 22], we can derive a second-order accurate difference formula in the normal direction, and finally derive a new FD formulation for Eq. (2). First we express u_4 and u_5 as Taylor series respectively at $x = 0, y = 0^+$ in the upper half space and $x = 0, y = 0^-$ in the lower half space as given in Eq. (11).

$$u_4 = \sum_{m=0}^{\infty} \frac{\Delta^m}{m!} u_{0^+}^{(m)}, \quad u_{0^+}^{(m)} \triangleq \left. \frac{\partial^m u}{\partial y^m} \right|_{(x=0, y=0^+)}, \quad u_5 = \sum_{m=0}^{\infty} \frac{(-\Delta)^m}{m!} u_{0^-}^{(m)}, \quad u_{0^-}^{(m)} \triangleq \left. \frac{\partial^m u}{\partial y^m} \right|_{(x=0, y=0^-)} \quad (11)$$

Second we can relate u_{0^+} and u_{0^-} to arbitrary order by the critical equation proposed in Chiou's work:

$$u_{0^+}^{(2n)} = \sum_{m=0}^n \binom{n}{m} \eta^{n-m} u_{0^-}^{2m}, \quad u_{0^+}^{(2n+1)} = \gamma \cdot \sum_{m=0}^n \binom{n}{m} \eta^{n-m} u_{0^-}^{2m+1} \quad (n = 0, 1, 2, \dots). \quad (12)$$

In Eq. (12), $\eta = k_2^2 - k_1^2$. With the help of Eq. (11) and Eq. (12), we may obtain a specific weighted sum of u_4 and u_5 as a FD approximation for u_{0^-}'' , which is formulated as:

$$u_{0^-}'' = \frac{u_4 + \gamma (1 + \eta \Delta^2/6) u_5 - [1 + \gamma + (3 + \gamma) \eta \Delta^2/6]}{\Delta^2 (1 + \gamma) (1 + \eta \Delta^2/6)/2} + O(\Delta^2). \quad (13)$$

Substituting Eq. (13) back into Eq. (2) and approximating $\partial^2 u / \partial x^2$ with a second-order accurate FD formula, we have:

$$\begin{aligned} c_0 \cdot u_0 &= c_I \cdot (u_2 + u_7) + c_u \cdot u_4 + c_d \cdot u_5, \\ c_0 &= 2(1 + \gamma) - (2 + \gamma) V_1^2/3 - (\gamma - 1) V_2^2/6 - \eta(1 + \gamma) V_2^2/12, \quad (\text{FD-AIC}) \\ c_I &= (1 + \gamma) (1 + \eta/6)/2, \quad c_u = 1, \quad c_d = \gamma(1 + \eta/6). \end{aligned} \quad (14)$$

In Eq. (14), $V_1 = n_1 k_0 \Delta$ and $V_2 = n_2 k_0 \Delta$. Note that Eq. (14) is developed without using any variation of the material-averaging approach. Back in 2000 [21], Chiou derived a high-order accurate FD formulation only for mode solving, applicable to 1-D or 1.5-D problems based on Eq. (12) and generalized Douglas scheme. However, the FD-AIC coefficients given by Eq. (14) we derived in this paper is a general 2-D formulation. Note that the four corner points u_1, u_3, u_6, u_8 , were not used in Eq. (14) for this horizontal interface case. In principle, this kind of FD-like formula can also be extended to cases with arbitrarily sloped interfaces. We may also obtain a full eight-point compact stencil using two-dimensional Taylor's expansion. The derivation process follows similar steps but with much more complex algebraic manipulation [23].

2.4. Fourier-Bessel Series Expansion (Hadley, 2002)

In [5], Dr. Hadley developed a high-order accuracy FD formulation for TE case only, holding true solely for points situated along the horizontal or vertical interface $(a, b, c) = (0, 1, 0)$. First he expanded the transverse magnetic fields by the Fourier-Bessel series (**FBS**) given by Eq. (15):

$$u(r, \phi) = \sum_{m=1}^{\infty} J_m(\xi_i r) \left[a_m^{(i)} \cos(m\phi) + b_m^{(i)} \sin(m\phi) \right]. \quad (15)$$

In Eq. (15), u represents either H_y or H_x , $\xi_i = \sqrt{k_i^2 - k_z^2}$, where $i = 1$ for $y > 0$ and $i = 2$ for $y < 0$. He then imposed the interface conditions, Eq. (3) and Eq. (4), on Eq. (15) for $r \in [0, \infty)$, and evaluated Eq. (15) at all FD grid points on the compact nine-point stencil. At the end, after extremely cumbersome derivation, it gave rise to a high-order accuracy FD (HO-FD) formula as given by Eq. (43) of Ref. [5]. The HO-FD formula exhibits sixth-order accuracy for the modal index and fourth-order accuracy for the small field component in problems without corners. However, due to the extreme complexity of the analytic analysis, it is very difficult to extend Hadley's work to an arbitrarily sloped interface. Nevertheless, thanks to Hadley's pioneering work in 2002 [5, 24], derivations of high-order accuracy FD formulations for uniform regions, interfaces and corners have been incorporated into high-accuracy eigenmode solvers for waveguides with rectangular cross-sections (for benchmark purposes).

3. LOCAL PLANE WAVE EXPANSION (LPWE) FORMULATION

In our previous work [6, 7], semi-analytic FD-like formulae LFE-9 and LFE-27 were derived for homogeneous Helmholtz equation by expanding the local field as a truncated Fourier-Bessel series for the 2-D case and a truncated spherical Fourier-Bessel series for the 3-D case. For cells containing an arbitrarily oriented dielectric interface we chose [25] to represent the local fields as a linear combination of select sets of plane wave solutions. The combined plane wave solutions automatically satisfy interface conditions given by Eqs. (3)–(4). The entire procedure is sequentially organized in three steps:

◆ Step 1: local plane wave solution

A combined plane wave solution $\psi_{\alpha \rightarrow \beta}$ is made of an incident wave ψ_{α}^i launched from medium α to medium β , a reflected wave $\psi_{\alpha\alpha}^r$ and a transmitted wave $\psi_{\beta\alpha}^t$.

$$\psi_{\alpha \rightarrow \beta} = \begin{cases} \psi_{\alpha}^i + \psi_{\alpha\alpha}^r, & \text{in medium } \alpha \\ \psi_{\beta\alpha}^t, & \text{in medium } \beta \end{cases}, \quad (16)$$

$$\psi_{\alpha}^i = e^{-j\mathbf{k}_{\alpha}^i \cdot \mathbf{r}'}, \quad \psi_{\alpha\alpha}^r = R_{\alpha\alpha} \cdot e^{-j\mathbf{k}_{\alpha}^r \cdot \mathbf{r}'}, \quad \psi_{\beta\alpha}^t = T_{\beta\alpha} \cdot e^{-j\mathbf{k}_{\beta}^t \cdot \mathbf{r}'},$$

where $(\alpha, \beta) = (1, 2)$ or $(2, 1)$. The wavenumber vectors \mathbf{k}_{α}^i , \mathbf{k}_{α}^r , \mathbf{k}_{β}^t and their components are given by:

$$\begin{aligned} \mathbf{k}_{\alpha}^i &= \hat{x}' p_{\alpha}^i + \hat{y}' q_{\alpha}^i, & p_{\alpha}^i &= k_{\alpha} \cos \theta, & q_{\alpha}^i &= k_{\alpha} \sin \theta, \\ \mathbf{k}_{\alpha}^r &= \hat{x}' p_{\alpha}^r + \hat{y}' q_{\alpha}^r, & p_{\alpha}^r &= p_{\alpha}^i, & q_{\alpha}^r &= -q_{\alpha}^i, \\ \mathbf{k}_{\beta}^t &= \hat{x}' p_{\beta}^t + \hat{y}' q_{\beta}^t, & p_{\beta}^t &= p_{\alpha}^i, & q_{\beta}^t &= (\alpha - \beta) \cdot \text{conj} \left\{ \sqrt{(k_{\beta})^2 - (p_{\alpha}^i)^2} \right\}. \end{aligned} \quad (17)$$

In Eq. (17), note that θ is the directional angle of the incident wave with respect to the $+x'$ direction, and therefore:

$$\begin{aligned} (i) \quad & -\pi < \theta < 0 \Leftrightarrow (\alpha, \beta) = (1, 2), \\ (ii) \quad & 0 < \theta < +\pi \Leftrightarrow (\alpha, \beta) = (2, 1). \end{aligned} \quad (18)$$

In the definition of q_{β}^t , we take the positive branch of $\sqrt{k_{\beta}^2 - (p_{\alpha}^i)^2}$ to avoid the exponentially-growing wave, and $\text{conj}\{\varpi\}$ refers to the complex conjugate of ϖ . The reflective coefficient $R_{\alpha\alpha}$ and transmission coefficient $T_{\beta\alpha}$ can be determined by the interface conditions Eq. (3) and Eq. (4), and are formulated as the Fresnel equations [19] given by Eq. (19)

$$R_{\alpha\alpha} = \frac{q_{\alpha}^i - \vartheta \cdot q_{\beta}^t}{q_{\alpha}^i + \vartheta \cdot q_{\beta}^t}, \quad T_{\beta\alpha} = 1 + R_{\alpha\alpha}, \quad \vartheta = \begin{cases} 1, & \text{for TE} \\ n_{\alpha}^2/n_{\beta}^2, & \text{for TM} \end{cases}. \quad (19)$$

◆ Step 2: construction of the matrix equation

We consider selected directions $\theta_m^{(1)}$ ($m = 1, 2, \dots, M_1$) for plane waves launched from medium 1, and directions $\theta_m^{(2)}$ ($m = 1, 2, \dots, M_2$) for waves launched from medium 2. The local field solution can be expressed as:

$$u(x', y') = \begin{cases} \sum_{m=1}^{M_1} c_m^{(1)} \cdot \left[\psi_1^i(x', y'; \theta_m^{(1)}) + \psi_{11}^r(x', y'; \theta_m^{(1)}) \right] + \sum_{m=1}^{M_2} c_m^{(2)} \cdot \psi_{12}^t(x', y'; \theta_m^{(2)}), & y' \geq 0 \\ \sum_{m=1}^{M_1} c_m^{(1)} \cdot \psi_{21}^t(x', y'; \theta_m^{(1)}) + \sum_{m=1}^{M_2} c_m^{(2)} \cdot \left[\psi_2^i(x', y'; \theta_m^{(2)}) + \psi_{22}^r(x', y'; \theta_m^{(2)}) \right], & y' < 0 \end{cases} \quad (20)$$

For the eight surrounding control nodes, we denote the interface-oriented coordinate of points belonging to medium i as $(x_n^{(i)}, y_n^{(i)})$, where $n = 1, 2, \dots, N_i$ and $i = 1, 2$. Of course, $N_1 + N_2 = 8$. Evaluating Eq. (20) at these surrounding points leads to the following matrix equation:

$$\mathbf{u} = \mathbf{\Psi} \mathbf{c} \Leftrightarrow \begin{bmatrix} \mathbf{u}_1 \\ \mathbf{u}_2 \end{bmatrix} = \begin{bmatrix} \mathbf{\Psi}_{11} & \mathbf{\Psi}_{12} \\ \mathbf{\Psi}_{21} & \mathbf{\Psi}_{22} \end{bmatrix} \begin{bmatrix} \mathbf{c}_1 \\ \mathbf{c}_2 \end{bmatrix}. \quad (21)$$

Here \mathbf{u} is the reordered vector \mathbf{u}_c of Eq. (7). Ψ is an 8-by- M matrix formed by four sub-matrices Ψ_{ij} which stands for the total field in medium i subject to the incident wave originating from medium j . $M = M_1 + M_2$, which is the total combined set of local plane-wave solutions. The subscripts of \mathbf{u} , \mathbf{c} denote the particular medium associated with the variables. Finally, we evaluate Eq. (20) at the central point $(x, y) = (0, 0)$ to obtain

$$u_0 = \mathbf{c}^T \boldsymbol{\psi}_0. \quad (22)$$

Here the M -by-1 vector $\boldsymbol{\psi}_0$ is simply the collection of each combined plane wave solutions evaluated at the central point.

◆ Step 3: LPWE compact stencil

To solve for Eq. (21) we first must choose M_1 and M_2 based on an empirical rule, which is dependent on the index contrast and the ratio between N_1 and N_2 . The directions of the incident plane waves are often chosen to be the Gauss quadrature directions. We choose $M = M_1 + M_2 = 8$ so that Ψ is an 8-by-8 square matrix. In cases we have tested, Ψ is invertible, hence we can express the weighted coefficients in terms of the eight surrounding local fields, which is:

$$\mathbf{c} = \Psi^{-1} \mathbf{U}. \quad (23)$$

Substituting Eq. (23) into Eq. (22) we have $u_0 = (\Psi^{-1} \mathbf{U})^T \boldsymbol{\psi}_0$, and thus the LPWE-based compact stencil vector \mathbf{d} , which is the reordered \mathbf{w} vector of Eq. (7), is given by:

$$\mathbf{d} = (\Psi^{-1})^T \boldsymbol{\psi}_0. \quad (\text{LPWE}) \quad (24)$$

Once we have the solution for the edge and corner points of a given square cell situated near a dielectric interface, the local field can be obtained with Eqs. (20) and (23). Thus, we have the reconstruction formula for the field defined everywhere within the cell from its eight surrounding points.

4. INVESTIGATION ON THE LOCAL ERROR OF LPWE COMPACT STENCILS

In this section we investigate the performance of the LPWE formulation by examining the characteristics of its relative local errors rather than studying certain bench-mark problems which produce global errors including grid dispersion errors and errors from the numerical transparent boundary conditions. We consider N_θ sets of plane wave solutions given by Eq. (16) and Eq. (17). The direction angle of the incident wave for the m -th set of plane wave solution is denoted by θ_m , $m = 1, 2, \dots, N_\theta$. As indicated by Eq. (18), negative values of θ_m represent the sets whose incident waves launched from medium 2 while positive values of θ_m is associated with waves launched from medium 1. In the error analysis, we set $0.01^\circ \leq |\theta_m| \leq 179.99^\circ$ to cover all incidental angles less than 89.99 degrees. Zero and 180 degree grazing angles are excluded to avoid divided by zero errors. Here we set N_θ to be a large number to ensure smoothly varying error curves.

For a plane wave solution corresponding to a particular θ_m , the exact values at the nine FD grid points, $u_{i,m}^{\text{exact}}$ ($i = 0, 1, 2, \dots, 9$), can be analytically calculated. The numerical value of the central field, $u_{0,m}^{\text{nume}}$ is computed using:

$$u_{0,m}^{\text{nume}} = \sum_{i=1}^8 w_i \cdot u_{i,m}^{\text{exact}}, \quad (25)$$

where stencil coefficients $\{w_i | i = 1, 2, \dots, 8\}$ are defined in Eq. (7). The relative local error is defined as:

$$\varepsilon_r^{(m)} = |u_{0,m}^{\text{nume}} - u_{0,m}^{\text{exact}}| / |u_{0,m}^{\text{exact}}|, \quad m = 1, 2, \dots, N_\theta. \quad (26)$$

Such a criterion allows us to focus solely on the error for FD-like compact stencils for the interface. n_H and n_L respectively denote higher and lower refractive indices. The dielectric contrast is defined as $n_{dc} = n_H/n_L$. The sampling density (number of sampling point per wavelength) N_λ is defined for the high index medium. The maximum relative local error or L_∞ -norm of $\varepsilon_r^{(m)}$ is defined as:

$$\varepsilon_{\max} = \text{Max}_{1 \leq m \leq N_\theta} \left\{ \varepsilon_r^{(m)} \right\}. \quad (27)$$

4.1. Relative Error V.S. Direction Angle

In Fig. 2 we plot local errors of LPWE versus three previously mentioned FD-like formulae for a centered horizontal interface $(a, b, c) = (0, 1, 0)$. The curves of relative error versus incident angle are plotted for low contrast ($n_{dc} = 1.5$) in Fig. 2(a) and for high contrast ($n_{dc} = 3.5$) in Fig. 2(b) at a spatial sampling density of ten points per wavelength. Note that FD-MatAve scheme maintains about 1% error except for the high contrast TM case. The FD-AIC maintains a relative error of less than 1% in all four cases. In general we can clearly see that LPWE scheme has an advantage of more than 20 dB over other formulae subject to an arbitrary incident plane wave for both low and high contrast cases. For aforementioned schemes, the numerical anisotropy is worse in the range of $-180^\circ < \theta < 0^\circ$ due to the existence of total internal reflection as waves launched from the high to the low index region. We also observed an interesting fact that only for TE cases, relative local errors are continuous across the two adjacent grazing angles coming from either region.

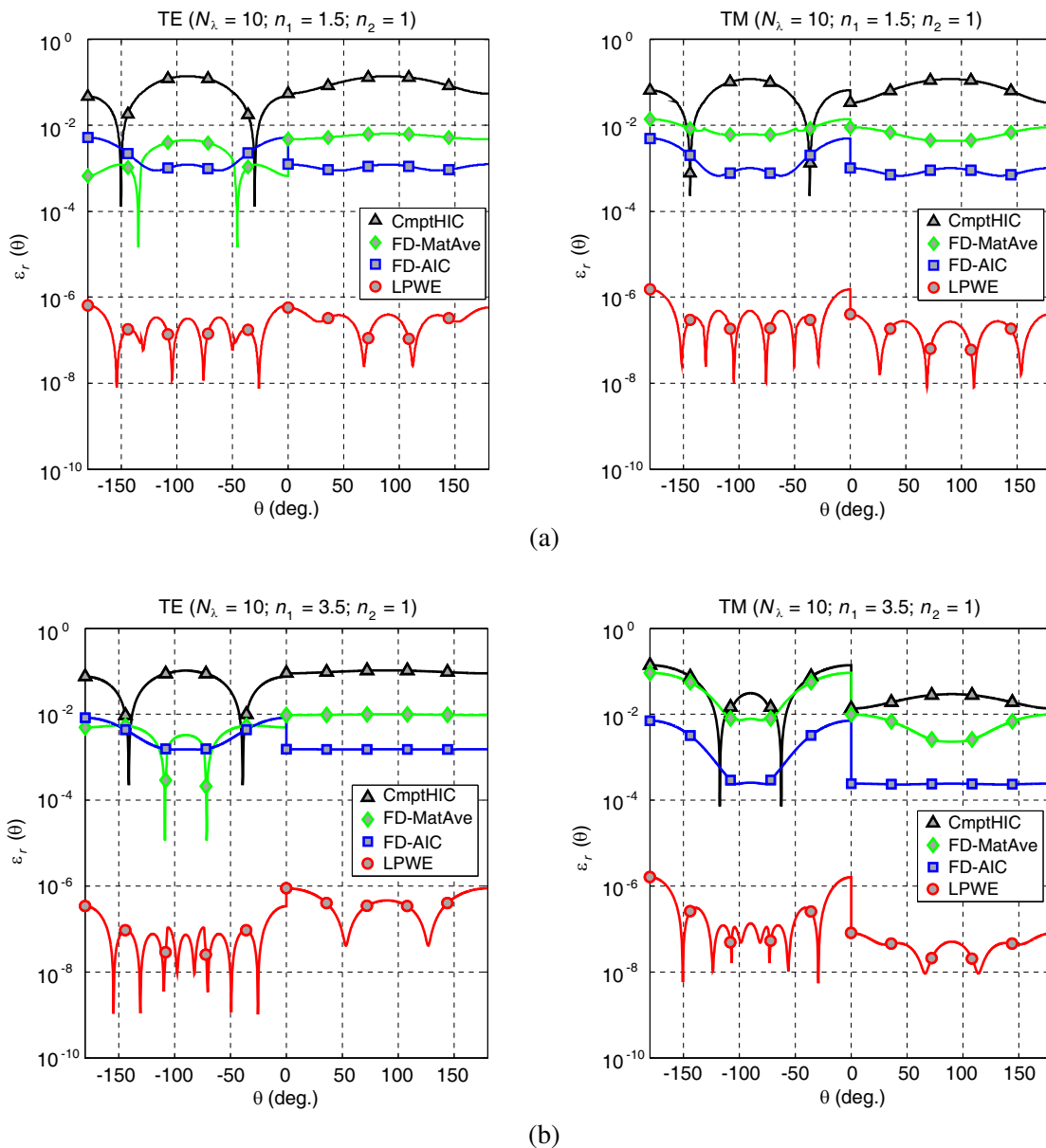


Figure 2. Comparison of relative local errors versus direction angles for various compact stencils sampled at 10 points per wavelength. (a) **Low contrast:** $n_{dc} = 1.5$, (b) **High contrast:** $n_{dc} = 3.5$.

4.2. Maximum Relative Error V.S. Sampling Density

Next we plot maximum relative errors versus sampling density N_λ . Low-contrast cases are plotted in Fig. 3(a) and high-contrast cases in Fig. 3(b).

From Fig. 3, we find the oversimplified formula CmpthIC converges very slowly as sampling density increases. The FD material-averaging scheme needs nine points per wavelength (for the higher index

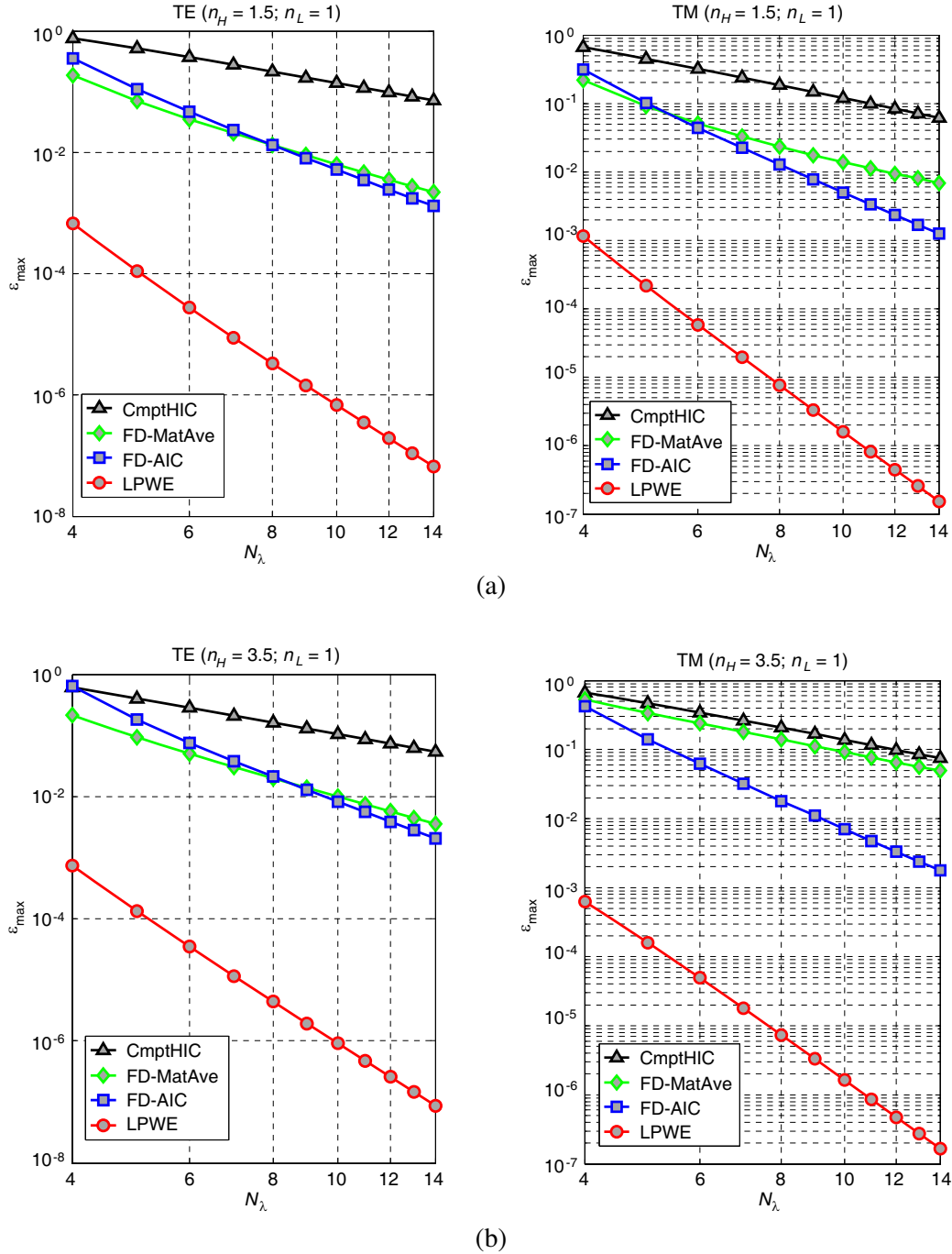


Figure 3. Comparison of maximum relative errors for various compact stencils as functions of sampling density for (a) low contrast and (b) high contrast. (a) **Low contrast:** $n_{dc} = 1.5$, (b) **High contrast:** $n_{dc} = 3.5$.

region) to achieve less than 1% relative local errors for TE cases. We need a $N_\lambda = 12$ to achieve the same level of accuracy for the TM case. As seen from Fig. 3(b) the effectiveness of FD-MatAve scheme decreases for TM cases with higher index contrasts. In contrast, FD-AIC is able to maintain low 1% maximum relative error at the cost of $N_\lambda = 9$ independent of index contrast or polarization. Obviously, the convergence rates of LPWE are much better and LPWE maintains a very little relative error in all cases considered. The slopes of these log-log curves in Fig. 3 are related to the convergence rate defined as:

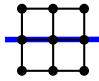
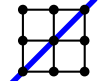
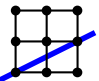
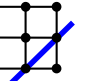
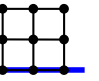
$$\xi = - \lim_{N_\lambda \rightarrow \infty} \Delta \log_{10}(\varepsilon_{\max}) / \Delta \log_{10}(N_\lambda). \quad (28)$$

Based on this definition, we find that $\xi_{\text{CmptHIC}} \approx 2$, $\xi_{\text{MatAve}} = 3$, $\xi_{\text{FD-AIC}} = 4$ and $\xi_{\text{LPWE}} \approx 7$ as shown in Fig. 3.

4.3. Maximum Relative Local Errors of LPWE V.S. Sampling Density for Various Inclined Interfaces

Now we investigate the characteristics of the maximum relative local error (**MRLE**) of the LPWE scheme for five types of line orientations, which are tabulated in Table 1. The types are classified by the (a, b, c) parameters Two horizontal (A , $E_>$, $E_<$), one diagonal (B) and two slanted ($C_>$, $C_<$ and $D_>$, $D_<$) line types are considered in this paper.

Table 1. Notations for various interface types.

(a, b, c)	(0, 1, 0)	(-1, 1, 0)	(-1, 2, 1)	(-1, 1, 1)	(0, 1, 1)
$n_1 > n_2$	A (6~8)	B (7~9)	C_{>} (4~6)	D_{>} (6~8)	E_{>} (8)
$n_1 < n_2$			C_{<} (5~6)	D_{<} (7~8)	E_{<} (8)
Layout					

For each variation, its interface geometry can be applied to other cases via a flip across the x -axis, y -axis or the x - y -axis. For example, the vertical interface can be obtained by applying x - y symmetry to the horizontal interface. The blue numbers in the parenthesis of Table 1 signify the corresponding convergence orders of the local error ξ defined in Eq. (28). As shown in Fig. 4, the **MRLE** of LPWE formulation is plotted as function of N_λ , the sampling density for each type of interface Note that the **MRLE** for the homogeneous nine-point formula, **FBS** based LFE-9 [6], given in Eq. (29), is also plotted to serve as a benchmark for two-medium LPWE compact stencils. Also note the relative local error for LFE-9 is evaluated for the high index region.

$$u_0 = \frac{J_4(V_s) \cdot (u_2 + u_4 + u_5 + u_7) + J_4(V) \cdot (u_1 + u_3 + u_6 + u_8)}{4[J_4(V_s) \cdot J_0(V) + J_4(V) \cdot J_0(V_s)]}. \quad (29)$$

In Eq. (29), $V_s = \sqrt{2}V$, and J_n is the Bessel function of the first kind of order n . LFE-9 exhibits eighth-order accuracy for the relative local errors as shown in Fig. 4, and the results are consistent with the LFE-9's local error formula given by Eq. (15) in [8].

Observing Fig. 4(a) and Fig. 4(b), LPWE stencils exhibits high-order accuracy for various dielectric contrast and for assorted line orientations. Even at the worst case scenario only four points per wavelength are required ($N_\lambda \geq 4$) to achieve less than 1% errors. And with a small increase of the sampling density to $N_\lambda \geq 4.5$, the **MRLE** decreases to an order of magnitude less. The convergence rate for the **MRLE** of assorted LPWE stencils is about fifth- to eighth-order accuracy in TE case, and about fourth- to ninth-order accuracy in TM case. We also note these errors are slightly more sensitive to interface layout in TM cases than those in TE cases.

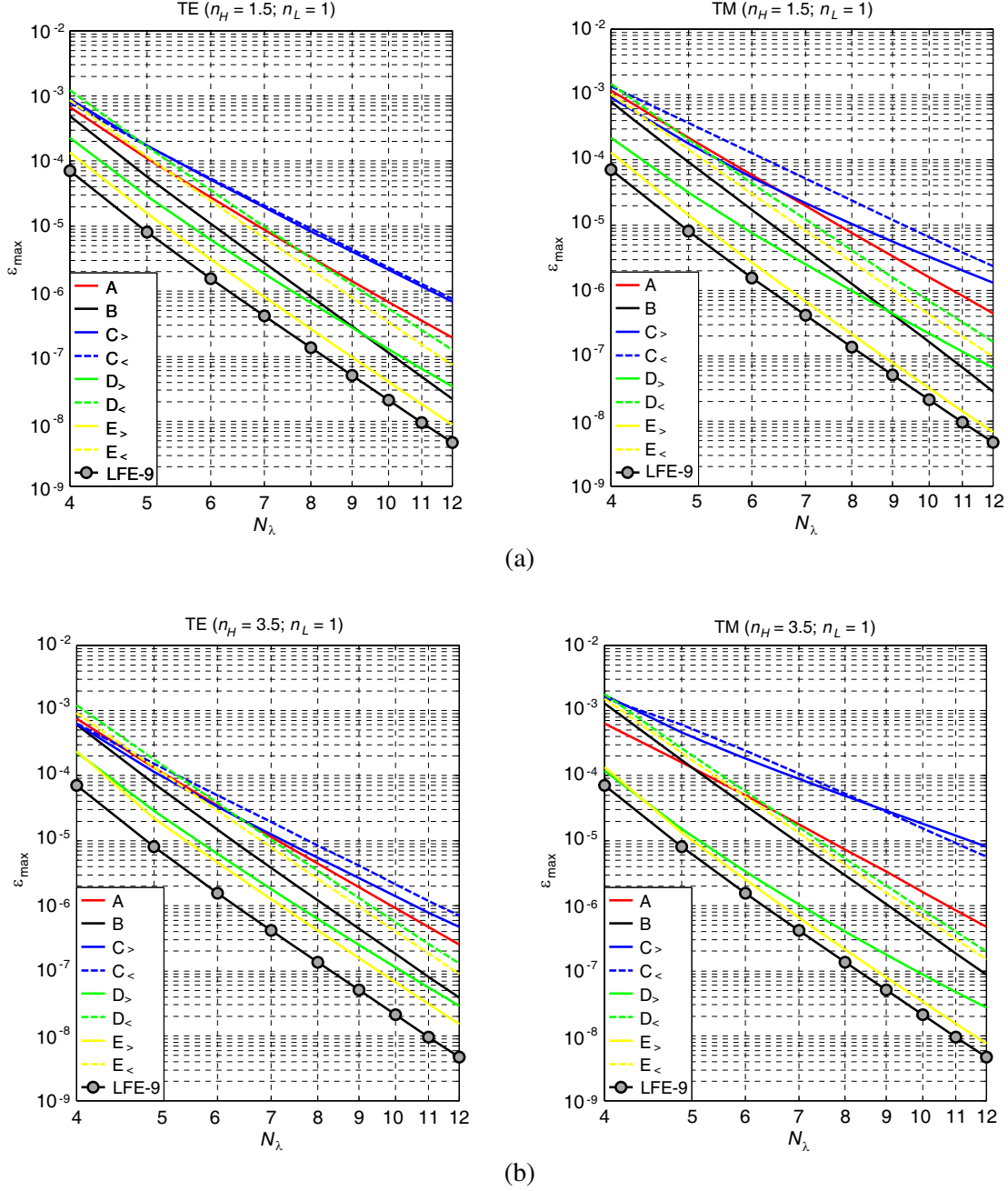


Figure 4. Performance investigation on LPWE scheme: maximum relative local error (ε_{\max}) versus sampling density (N_λ) for (a) low contrast and (b) high contrast scenarios. (a) **Low contrast** ($n_{dc} = 1.5$), (b) **High contrast** ($n_{dc} = 3.5$).

5. DISCUSSIONS

The effectiveness of the stencil coefficients for LPWE-based CLF schemes are crucially dependent on the following parameters:

- (I) M_i , $i = 1, 2$: The number of plane waves launched from medium i .
- (II) $\theta_m^{(i)}$, $i = 1, 2$: The directions angles of plane waves launched from medium i .

Keep in mind that we have only eight constraints (Eq. (28)).

When $M_1 + M_2 > 8$ we have an under-determined system of linear equations. The solutions to Eq. (21) are not unique and we have to resort to linear algebra methods to obtain a “good” solution. We have discovered that the local error can be reduced by using larger M_i pairs with uniformly distributed $\theta_m^{(i)}$. We also note that the accuracy increases very slowly as the sum of M_1 and M_2 exceed the low hundreds. In another approach we may choose a suitable $\theta_m^{(i)}$, for example the Gauss quadrature directions, to obtain satisfactory coefficients while $M_1 + M_2 = 8$. The optimized choice of M_i and $\theta_m^{(i)}$ for general cases is still an open question. Finally, unlike other stencils, the computed LPWE coefficients are complex numbers with tiny imaginary parts. To conclude this section we summarize the characteristics of LPWE and other FD-like formulae in Table 2.

Table 2. Comparison of various FD-like schemes for Helmholtz interface problems.

Scheme	Stencil	Formula	C.O.*	Characteristics
CmptHIC	3-point	Eq. (8)	2	An intuitive formula.
FD-MatAve	5-point	Eq. (10)	3	An easily implemetable method for all types of interfaces. Performance is better for TE cases. Not very good for cases with high index contrasts.
FD-AIC	5-point	Eq. (14)	4	Accurate enough for both TE and TM cases. Peformance slightly affected by dielectric contrasts. May be extended to arbitrarily-sloped interfaces.
Hadley	9-point	Ref. [24]	7	Tedious derivation. Highly accurate but only for the horizontal TE case. Used as a benchmark mode solver for rectangular waveguides.
LPWE	9-point	Eq. (24)	4–8	Highly accurate for wide index contrasts and both polarizations. Flexible for arbitrary types of interfaces.

*C.O. = convergence order of the maximum relative local error

6. CONCLUSIONS

In this paper we present LPWE formulation for deriving FD-like compact stencils for points near or on a dielectric interface. The effectiveness of LPWE coefficients is dependent on the particular choice of modeling parameters, namely the number of local plane waves and their incident angles. We numerically demonstrate that for various types of straight interfaces with low to high dielectric contrasts, our LPWE scheme maintains between fourth to eighth-order (local) accuracy for both TE and TM polarizations. Compared with existing compact stencils derived from either the FD-MatAve or the FD-AIC schemes, LPWE enjoys an accuracy advantage of more than 20 dB. We also numerically determine that we have fourth to eighth-order accuracy in LPWE stencil local errors. Moreover, the overall performance of our proposed LPWE-based compact stencils for Helmholtz equation with a planar dielectric interface is on par with the known optimal **FSB**-based LFE-9 formula for homogeneous media. This is a crucial step toward obtaining high-order accurate, numerical solutions to the Helmholtz equation of complex passive EM/optical waveguide devices.

ACKNOWLEDGMENT

We are grateful for the support of the Ministry of Science and Technology of the Republic of China under the contracts 102-2221-E-110-073-MY3.

REFERENCES

1. Shin, C. and H. Sohn, "A frequency-space 2-D scalar wave extrapolator using extended 25-point finite difference operator," *Geophysics*, Vol. 63, No. 1, 289–296, 1998.
2. Singer, I. and E. Turkel, "Sixth order accurate finite difference schemes for the Helmholtz equation," *Journal of Computational Acoustics*, Vol. 14, 339–351, 2006.
3. Tsukerman, I., "A class of difference schemes with flexible local approximation," *Journal of Computational Physics*, Vol. 211, No. 2, 659–699, 2006.
4. Fernandes, D. T. and A. F. D. Loula, "Quasi optimal finite difference method for Helmholtz problem on unstructured grids," *Int. J. Numer. Meth. Engng.*, Vol. 82, 1244–1281, 2010.
5. Hadley, G. R., "High-accuracy finite-difference equations for dielectric waveguide analysis I: Uniform regions and dielectric interfaces," *J. Lightwave Technol.*, Vol. 20, No. 5, 1210–1218, 2002.
6. Chang, H.-W. and S.-Y. Mu, "Semi-analytical solutions of 2-D homogeneous Helmholtz equation by the method of connected local fields," *Progress In Electromagnetics Research*, Vol. 109, 399–424, 2010.
7. Chang, H.-W. and S.-Y. Mu, "Semi-analytical solutions of the 3-D homogeneous Helmholtz equation by the method of connected local fields," *Progress In Electromagnetics Research*, Vol. 142, 159–188, 2013.
8. Mu, S.-Y. and H.-W. Chang, "Theoretical foundation for the method of connected local fields," *Progress In Electromagnetics Research*, Vol. 114, 67–88, 2011.
9. Mu, S.-Y. and H.-W. Chang, "Dispersion and local-error analysis of compact LFE-27 formula for obtaining sixth-order accurate numerical solutions of 3D Helmholtz equation," *Progress In Electromagnetics Research*, Vol. 143, 285–314, 2013.
10. Chang, H.-W., Y.-H. Wu, and W.-C. Cheng, "Hybrid FD-FD analysis of crossing waveguides by exploiting both the plus and the cross structural symmetry," *Progress In Electromagnetics Research*, Vol. 103, 217–240, 2010.
11. Chang, H.-W. and Y.-H. Wu, "Analysis of perpendicular crossing dielectric waveguides with various typical index contrasts and intersection profiles," *Progress In Electromagnetics Research*, Vol. 108, 323–341, 2010.
12. Chang, H.-W., W.-C. Cheng, and S.-M. Lu, "Layer-mode transparent boundary condition for the hybrid FD-FD method," *Progress In Electromagnetics Research*, Vol. 94, 175–195, 2009.
13. Stern, M. S., "Semivectorial polarised finite difference method for optical waveguides with arbitrary index profiles," *IEE Proceedings — J. Optoelectronics*, Vol. 135, No. 1, 56–63, 1988.
14. Vassallo, C., "Improvement of finite difference methods for step-index optical waveguides," *IEE Proceedings — J. Optoelectronics*, Vol. 139, No. 2, 137–142, 1992.
15. Yamauchi, J. and J. Shibayama, "Modified finite-difference formula for the analysis of semivectorial modes in step-index optical waveguides," *IEEE Photonics Technology Letters*, Vol. 9, No. 5, 1997.
16. Taflov, A. and S. C. Hagness, *Computational Electrodynamics: The Finite-difference Time-domain Method*, 3rd Edition, Artech House, Norwood, MA, 2005.
17. Peterson, R. and Mittra, *Computational Method for Electromagnetics*, IEEE Press, 1998.
18. Rao, K. R., J. Nehrbass, and R. Lee, "Discretization errors in finite methods: Issues and possible solutions," *Comput. Methods Appl. Mech. Engrg.*, Vol. 169, 219–236, 1999.
19. Durdević, D. Z., "Finite-difference modeling of dielectric interfaces in electromagnetics and photonics," *Infoteh.-Jahorina.*, Vol. 9, 697–701, 2010.
20. Ishimaru, A., *Electromagnetic Propagation, Radiation, and Scattering*, Prentice Hall, Englewood Cliffs, N.J., 1991.

21. Chiou, Y.-P., Y.-C. Chiang, and H.-C. Chang, "Improved three-point formulas considering the interface conditions in the finite-difference analysis of step-index optical devices," *J. Lightwave Technol.*, Vol. 18, No. 2, 2000.
22. Chiou, Y.-P. and C.-H. Du, "Arbitrary-order interface conditions for slab structures and their applications in waveguide analysis," *Optics Express*, Vol. 18, No. 3, 4088–4102, 2010.
23. Chiou, Y.-P., Y.-C. Chiang, et al., "Finite-difference modeling of dielectric waveguides with corners and slanted facets," *J. Lightwave Technol.*, Vol. 27, No. 8, 2077–2086, 2009.
24. Hadley, G. R., "High-accuracy finite-difference equations for dielectric waveguide analysis II: Dielectric corners," *J. Lightwave Technol.*, Vol. 20, No. 5, 1219–1231, 2002.
25. Chang, H.-W. and S.-Y. Mu, "Compact 2D stencils for inhomogeneous Helmholtz equation based on method of connected local fields," *Computational Electromagnetics, ICCEM 2015*, 215–217, 2015.